HHS Public Access

Author manuscript

Nat Immunol. Author manuscript; available in PMC 2015 September 01.

Published in final edited form as:

Nat Immunol. 2015 March ; 16(3): 296–305. doi:10.1038/ni.3095.

Switched-memory B cells remodel B cell receptors within secondary germinal centers

Louise J. McHeyzer-Williams[#], **Pierre J. Milpied**[##], **Shinji L. Okitsu**[§], and **Michael G. McHeyzer-Williams**[‡]

Department of Immunology and Microbial Science The Scripps Research Institute, La Jolla CA 92037

[#] These authors contributed equally to this work.

Abstract

Effective vaccines induce high-affinity memory B cells and durable antibody responses through accelerated mechanisms of natural selection. Secondary changes in antibody repertoires after vaccine boosts suggest progressive B cell receptor (BCR) re-diversification, but underlying mechanisms remain unresolved. Here integrated specificity and function of individual memory B cell progeny reveal ongoing evolution of polyclonal antibody specificities through germinal center (GC) specific transcriptional activity. At the clonal and sub-clonal levels, single cell expression of *Cd83* and *Pol*□ segregates the secondary GC transcriptional program into 4 stages that regulate divergent mechanisms of memory BCR evolution. These studies demonstrate that vaccine boosts re-activate a cyclic program of GC function in switched-memory B cells to remodel existing antibody specificities and enhance durable immune protection.

Antibody-mediated immune protection relies heavily on the development of high-affinity memory B cells and long-lived plasma cells (PCs). Priming with protein antigens induces antigen-specific follicular helper T (T_{FH}) cells needed to initiate primary-response germinal center (GC) reactions [1-3]. Following cognate contact, cohorts of antigen-primed B cells form GC microenvironments to expand and diversify germ-line encoded B cell receptors (BCR) [3-5]. Dynamic imaging has recently provided a real-time framework for understanding GC-based evolution of antigen-specific BCR recognition[6-8]. Location-based labeling of GC B cells [9] and more recently labeled GC T_{FH} cells [10], have provided a new level of understanding for the regulation of GC B cell fate. However, the strict requirement of this spatial organization [11], the sequence of GC B cell functions and the dynamics of evolutionary processes regulating memory B cell fate and function at antigen recall remain unclear.

[‡]Corresponding author. mcheyzer@scripps.edu.
[#]Current address Center d'Immunologie de Marseille-Luminy. Marseilles, France
[§]Current address EMD Serono Research and Development Institute, Billerica MA 01821 USA

Author Contributions

L.M.W., P.J.M. and M.M.W. designed, performed experiments, analyzed the data and wrote the paper. S.L.O. designed and performed the experiments in Supplementary Fig 1c.

Clonal BCR diversification and selection of higher-affinity variants are the dominant mechanisms driving evolution of antigen-specific B cell memory [3-5, 12]. Somatic hypermutation (SHM) diversifies antigen-specific BCR in progeny of rapidly proliferating GC B cells [3, 4, 12, 13]. Clonal progeny expressing variant BCR scan follicular dendritic cell (FDC) networks [6-8] with varying ability for antigen uptake, processing and presentation. In this manner, GC B cells with greater access to antigen make stronger productive contacts with GC T_{FH} cells [14], proliferate more extensively and further diversify the preferred and selected antigen-specific BCR [15]. GC containment and the cyclic progression of BCR diversification can be observed through clonal organization of GC B cell repertoire analysis [16, 17]. However, it remains important to connect these multiple attributes within individual antigen-specific GC B cell clones to understand how specialized GC-specific transcriptional programs drive ongoing BCR re-diversification.

Modifying antigen-specific B cell memory at recall is central to antibody-mediated immune protection. Classic studies demonstrated the progressive increase in memory BCR diversity with antigen recall [18, 19]. While transfer studies indicated that memory B cells expanded without BCR re-diversification [20], they also suggested that 'selective recruitment' of affinity-matured memory B cells into PC differentiation could explain ongoing antibody repertoire maturation without re-initiation of the GC reaction. Prime-boost studies using protein antigens [21, 22] and transfer models relying on particular antigens [23, 24] reported similar skewing of switched-memory responses towards PC production. Differential Bach-2 expression in switched-memory B cells suggested an intrinsic molecular basis for PC skewing at recall [25]. In contrast, many recent BCR repertoire studies of circulating human memory B cells [26-33] observe clonal expansions of switched-memory B cells with BCR that expressed shared and unique mutations. These data suggest an alternate 'memory BCR re-diversification' model that predicts local secondary GC formation and ongoing function with extended exposure to antigen or the vaccine boost. More recent adoptive transfer studies [34, 35] provide supportive evidence for this alternate model, but there remains little insight into local mechanisms.

Here, we developed a high-resolution cellular and molecular strategy to monitor antigen-specific GC B cell fate within intact primed animals expressing a polyclonal immune system. Our findings demonstrate that antigen recall elicits robust secondary GC reactions in large cohorts of switched-memory B cells. Secondary GC B cells reinitiate a cyclic GC transcriptional program to diversify memory BCR repertoires with ongoing antigen-driven selection at the clonal and sub-clonal level. Persistent primary GCs were not required for secondary GC formation and multiple lines of evidence demonstrate that switched-memory B cells are the major precursors in intact primed animals. These studies identify the local cellular targets and molecular mechanisms that drive ongoing switched-antibody re-diversification at recall.

RESULTS

Robust secondary GC formation upon antigen recall

Single cell mapping of GC B cell fate within the clonal progeny of memory B cells is a powerful means for monitoring antigen-specific differentiation *in vivo*. In the absence of a

clear understanding of memory T_{FH} organization and function, it is prudent and necessary to assess recall responses without the use of adoptive transfer. Here, we used hapten-protein (NP-KLH) prime-boost immunization to isolate antigen-specific ($V_L\lambda1$ NP^+) memory-response B cells directly *ex vivo* [36-38]. After the boost, there was robust emergence of class-switched (IgM^-IgD^-) antigen-specific GC ($GL7^{hi}CD38^{lo}$) B cells expressing Bcl-6 protein and low amounts of CD62L (**Fig. 1a**). Local emergence of these cells after the boost was not dependent on the presence of adjuvant (**Fig. 1b**). Distinct IgD^- GC structures containing $CD21^+CD35^+$ follicular dendritic cell (FDC) networks, AID, Bcl-6 and GC-localized $CD4^+$ T_{FH} cells were evident by antibody labeling in tissue sections (**Fig. 1c**). Based on flow cytometry and antigen binding, carrier protein-specific memory B cells also formed robust switched secondary GC in these draining LN at both timepoints after the boost (**Fig. 1d**). Based on the same set of markers and cellular dynamics described above, changes in priming adjuvant (**Supplementary Fig. 1a**), priming dose (**Supplementary Fig. 1b**) or time after priming (>6months; not shown) generated similar frequencies and levels of GC B cells after the boost. Therefore, local antigen re-challenge drives robust GC reactions containing large numbers of switched antigen-specific GC B cells with broadly similar spatial organization *in situ*.

Class-switched B cells re-diversify BCR within secondary GC

To measure ongoing BCR diversification *in vivo*, we connected the information for phenotype and antibody repertoire for >500 individual switched antigen-specific B cells over the course of the secondary response. $V_L\lambda1$-$V_H186.2$ expressing polyclonal B cells with numerous unique junctional sequences dominated the response in vivo (**Supplementary Fig. 2**). We used dendrogram displays of near-neighbor sequence alignment [39] to depict the scale of polyclonal relatedness within responding antigen-specific B cells sorted from separate timepoints after initial priming or the secondary boost. Changes between primary-response GC, memory B cells before recall and GC B cells after the boost, demonstrated high amounts of BCR diversification through polyclonal outgrowth within secondary GC reactions (**Fig. 2a**). Linear distance from the predicted root of each dendrogram (**Fig. 2b**), changes in the frequency of mutations per GC B cell (**Fig. 2c**) and the distribution of aa changes (**Fig. 2d**) all indicated ongoing memory BCR diversification within switched secondary GC B cells. Soluble antigen boost induced shorter measured distance to root (Fig. 2b) and lower numbers of mutations per GC B cell (Fig. 2c) than found with adjuvant. As such, the single cell analysis quantifies increased BCR diversification in polyclonal switched-memory BCR repertoires induced by the vaccine boost and influenced by addition of exogenous adjuvant.

Transcriptional programs expressed by secondary GC B cells

Recent imaging strategies have used location to define zonal changes in gene expression that accompany progressive GC B cell function [3, 9]. Here we used high-order 96-plex single cell RT-qPCR to quantify gene expression in individual antigen-specific B cells (**Supplementary Fig. 3**). An increased percentage of switched secondary GC B cells from day 8 after the boost expressed genes encoding GC guidance and survival cues (*Cxcr5*, *Cxcr4*, *Baffr*, *Il21r)*, indicators of proliferation (*Mki67*, *Pcna*), BCR diversification (*Aicda*,

Polh), DNA repair and transcriptional regulators (*Bcl6*, *Foxo1*, *E2a*, *Id3)* and co-modifiers of T-B contact (*Ly75*, *Slamf1*, *CD24a*, *Fas*)(**Fig. 2e, upper panel**) compared to memory B cells before the boost. These indicators of GC-specific transcriptional programing were induced rapidly after the boost in GC B cells with high frequencies maintained at the single cell level across the first week (**Fig. 2e, lower panel**).

Individual switched-memory B cells were mostly quiescent displaying negligible *Aicda* expression and low frequencies of cells with *Bcl6* and *Mki67 mRNA* (**Fig. 2f**). In contrast, expression of *Aicda*, *Bcl6* and *Mki67* mRNA indicated global GC transcriptional activities that persisted 70 days after initial priming, and were also detected on day 4 and 8 after recall within recently expanded individual secondary GC B cells. In the absence of adjuvant at the boost, *Aicda*, *Bcl6* and *Mki67* mRNA are present at similar levels on a per GC B cell basis at the same timepoints following the boost. These data demonstrate re-initiation and ongoing GC-specific transcriptional activities within secondary GC B cells that serve to re-diversify the switched BCR repertoires of polyclonal memory B cells.

Cyclic GC transcriptional programs assort across 4 stages

The GC cycle involves sequential transcriptional changes and coordinated cellular function to promote and enhance BCR diversity. To interrogate the coordinated programming of multiple progressive GC B cell functions, we calculated the combinatorial associations of gene expression among individual antigen-specific GC B cells. Principal component analysis (PCA) of gene expression from all secondary GC B cells segregated a subset of GC-associated activities into putative LZ (eg *Cd83, Slamf Cd86, IL21r and Myc*,) and DZ (eg *Polh, Cxcr4*, *Mki67* and *Cd24a*) sub-compartments (**Supplementary Fig. 4 & 5**). We then used the dimensionality reduction algorithm t-SNE (t-distributed stochastic neighbor embedding)[40] to display varied differential expression for a subset of known GC activities [9] (*Cd79b*, *Bcl6*, *Aicda*, *Mki67*, *Polh*, *Cd83* and *Cxcr4*) across the secondary GC B cells after the boost (**Fig. 3a**). With few exceptions, switched GC B cells clustered into four major regions of bivariate t-SNE plots (separately designated as Stages 1 to 4) representing clustered and segregated transcriptional activity in single GC B cells (**Fig. 3b**).

From the selected set of genes, *Cd83* and *Pol*□ mRNA contributed most clearly to the clustering of individual GC B cells (**Fig. 3c**). Based on the predicted functions of *Cd83* and *Polh* [41, 42], we propose four separate stages of GC transcriptional activity that assort GC B cells within the four regions on the tSNE plots. Lack of *Polh* expression suggested no hypermutation machinery placing $Cd83^{-}$ $Polh^{-}$ cells in a LZ compartment designated as Stage 1. Increased antigen presentation with potential T-B contact associated with *Cd83* expression placed $Cd83^{+}Polh^{-}$ GC B cells into a separate LZ compartment designated as Stage 2. Expression of *Polh* indicated BCR diversification potential in the DZ with $Cd83^{+}Polh^{+}$ GC B cells representing recent arrivals into a DZ compartment designated as Stage 3. Loss of Cd83 then places the $Cd83^{-}Polh^{+}$ DZ compartment, more distant from recent T-B contact and then designated as Stage 4. Finally, loss of *Polh* expression with LZ re-entry before expression of *Cd83* would restart the cycle of GC transcriptional programing.

Across the four stages of the proposed GC cycle *Cxcr4* and *Mki67* levels per GC B cell skewed towards GC cells in the DZ (**Fig. 3d; upper panels**). Higher proportions of cells within stages 2 and 3 expressing *Il21r*, *Slamf1* (**Fig. 3d, middle panels**) and the predicted relationship between cells across the 4 stages based on coordinated *Cd83*, *Polh*, *Aicda* and *Mki67* supported the cyclic behavior of GC B cells in the proposed model (**Supplementary Fig. 6**). Furthermore, LZ re-entry between stages 4 and 1 of the GC cycle was accompanied by decreased *Cxcr4*, *Mki67*, *Cd24a* and increased *Cd38* expression (Fig. 3e & 3f; bottom panels). Antigen presentation and T-B contact in the LZ between stages 1 and 2 was accompanied by lowered *Cxcr4*, *E2a* expression and increased *Icosl*, *IL21r*, *Baffr*, *Slamf1*, *Cxcr5* (Fig. 3e & 3f; top panels). DZ entry after T-B contact between stages 2 and 3 was associated with increased expression of *Aicda*, *Pcna*, *Mki67*, *Cxcr4*, *Ly75* and *CD24a* (Fig. 3e second panel & Fig. 3f fourth & fifth panels). Finally, extended diversification in the DZ between stages 3 and 4 was accompanied by continued high expression of *Aicda*, *Mki67*, *Cxcr4* and decreased *Myc*, *Ly75* and *Il10rb* (Fig. 3e; third panel). These more extended analyses of coordinated single cell gene expression are consistent with the proposed cyclic progression of GC B cell transcriptional programing.

Sub-clonal adaptive radiation of switched BCR repertoires

Ongoing selection of diversified antigen-specific BCR within individual GC B cell clones provides direct evidence of GC function *in vivo* [16, 17]. To reveal the evolutionary dynamics of secondary GC function, we directly connected the single cell gene expression to clonal BCR repertoire analysis in an integrated single cell analysis (iSCA). We performed iSCA on antigen-specific GC B cell clones isolated from individual LNs from day 4 and 8 after the boost and defined by unique CDR3 junctions (>10 members per clone; n = 9). The index sort analysis of the clones indicated that levels of antigen binding, light chain expression and surface phenotype distribution was similar to the total population of GC B cells (**Fig. 4a;** clone G displayed against contour plots for total population). Furthermore, each clone contained sub-clonal members distributed across all 4 stages of the GC cycle (**Fig. 4b**). Fewer sub-clonal members resided in stages 2 and 3 of the GC cycle (Fig. 4b) consistent with the loss of unselected LZ GC B cell variants and exit from the GC after T-B contact.

Sub-clonal distribution of BCR mutations reveals GC evolutionary dynamics. We next assessed whether individual GC clones converge towards a single variant on a subclonal branch or diverge across multiple options to progress diversification in many branches independently. Sequence alignment and near neighbor analysis of clonal BCR repertoires displayed in radial phylograms outlined sub-clonal GC B cell activity (**Fig. 4c**; clone H & G). Based on these related distributions of mutational variants, there was evidence for multiple divergent branches of sub-clonal variants that had re-expanded after selection and re-diversified in separate clusters of GC clonal progeny (Fig. 4c). Separate sub-clonal clusters also contained individual members of the clone that distributed across multiple different GC transcriptional stages as defined by the tSNE grouping of 4 stages as described above (**Fig. 4d**). In a separate representation of clonal data, we tabulated multiple facets of cellular and molecular secondary GC B cell activity independent of BCR sequence alignment to highlight similar and unique GC programs expressed at the sub-clonal level (**Fig. 4e**; clone G).

Taken together, these results demonstrate re-diversification of the mutated and class-switched BCR repertoire in antigen-specific secondary GC B cells. These data also indicate that antigen drives the selection of sub-clonal BCR variants within secondary GC. Furthermore, the segregation of individual GC B cells across the 4 stages of the GC cycle in separate intra-clonal clusters indicates the permissive, ongoing and divergent nature of antigen-specific secondary GC B cell evolution. These results favor a divergent mechanism of evolution and reveal the dynamics of sub-clonal adaptive radiation within secondary GC for switched-memory BCR repertoires.

De novo secondary GC formation

Local LN GC reactions can persist at low levels for extended periods [43] and activated B cells can join pre-existing GC [44]. To investigate whether secondary GC reactions can arise de novo following antigen recall regimes described above, we focused analysis on remote cervical LNs that contained no evidence of persistent primary GC (**Fig. 5a**). In these primed animals, an intravenous boost of antigen without adjuvant induced equivalent frequencies of antigen-specific GC B cells in both local LNs draining the initial priming site and remote LNs. Next, using blocking anti-CD40L antibodies, we ablated pre-existing GCs in similarly primed animals, an intravenous antigen boost produced equivalent frequencies of GC B cells compared to untreated controls (**Fig. 5b**). In both sets of experiments, antigen-specific memory B cells are the most likely precursors of the local secondary GC response at recall. Therefore, the vaccine boost can induce de novo GC reactions, even at lowered local levels of antigen, and does not require adjuvant or the presence of persistent primary-response GC reactions.

Switched memory B cells can form GC on transfer

We next used adoptive transfer models to examine the origins of secondary GC precursors. Day 70 after priming with NP-KLH, switched-memory B cells ($IgM^{-}IgDCD19^{+}GL7^{-}$) were isolated without using antigen-specificity and co-transferred with $CD4^{+}$ $CD44^{hi}$ T cells as a source of memory T_H cells into *Rag-1*$^{tm1/Mom}$ recipient mice (**Supplementary Fig. 7a**). Day 14 after recall, high numbers of non antigen-specific $CD38^{-}GL7^{+}$ GCs were observed in the spleens of recipient animals, however the antigen-specific ($NP^{+}\lambda^{+}$) GC response ($CD38^{-}GL7^{+}$) was variable (not shown). To overcome the variability within the antigen-specific compartment, we included naïve non-specific B cells (MD4 BCR transgenic B cells specific for HEL) at transfer. This non-specific 'filler' cell effect resulted in antigen-specific switched-memory B cells consistently producing secondary GC responses at recall (**Supplementary Fig-7b & 7c**). To interrogate memory function under more physiological conditions than transfer into *Rag-1*$^{tm1/Mom}$ recipients, we transferred 3-5 × 10^3 NP^{+} switched-memory B cells ($IgM^{-}IgDCD138^{-}CD19^{+}CD38^{+}$) into naïve syngeneic WT recipients and observed antigen-specific ($NP^{+}\lambda^{+}$) Bcl-6 expressing GC B cells in spleens of recipients 7 days after transfer and challenge (**Fig. 6a**). As expected, isolated $CD38^{-}GL7^{+}$ antigen-specific GC B cells transferred in this model were not recovered and did not respond to immunization (not shown). In a third model using transfer of NP+ switched-memory B cells transfer into unconditioned the MD4 BCR transgenic as recipient, we observed substantial antigen-specific ($NP^{+}\lambda^{+}$) $Bcl6^{+}$ GC B cell compartment (**Fig-6b**). Thus, under all

conditions tested, switched-memory B cells displayed the potential to form secondary GC reactions upon antigen recall.

IgM^+ memory B cells can form GC upon transfer and re-activation with repetitive particulate antigens [23]. Transferring equivalent numbers ($3\text{-}5 \times 10^3$) of NP^+IgM^+ and switched-memory B cells into unconditoned wild-type recipients produced similar expansion of $NP^+\lambda^+$ memory B cells ($CD138^-$ $CD38^+GL7^-$) in spleens of recipients day 7 after recall (**Fig. 6a**). Consistent with previous findings [25], a minority of transferred memory B cells lost IgM expression after recall (**Fig. 6a**). Furthermore, NP^+IgM^+ memory B cells produced 10-fold fewer GC B cells than observed with switched-memory counterparts in similar unconditioned recipients (**Fig. 6a**). Therefore, some IgM^+ memory B cells can form secondary GC [23, 35], but switched-memory B cells have the dominant precursor potential for secondary GC formation in this model.

Switched memory B cells are predominant secondary GC precursors

We next measure the dynamics and diversity of the antigen-specific IgM^+ B cell response to antigen recall in the intact primed animal. TLR4 agonist adjuvant induced high amounts of IgG2a and IgG2b class-switch but also promoted NP^+ $V_L\lambda1^+$ IgM^+ memory B cells (**Fig. 7a**). However, based on Bcl-6 expression, very few of these antigen-specific IgM^+ memory B cells resided within persistent primary-response GCs in the LNs at day 70 after priming and before recall (Fig. 7a). Furthermore, $V_H186.2$ IgM^+ BCR from these IgM^+ memory B cells were largely unmutated or expressed related but unmutated non-$V_H186.2$ genes. The low mutation rate of IgM^+ memory B cells is consistent with a GC independent pathway for this unswitched memory compartment [45, 46]. After recall, antigen-binding $V_L\lambda1^+$ IgM^+ memory B cells expanded predominantly into the antigen-specific $CD138^+$ memory-response PC compartment, while <2% of the total antigen-specific cells expressed the $GL7^{hi}CD38^{lo}$ GC phenotype (**Fig. 7b**). Thus, as seen in the adoptive transfer, antigen-specific IgM^+ memory B cells had little secondary GC forming potential within the intact primed animal.

At the molecular level, class switch recombination (CSR) leaves switch circle transcripts within individual cells that have recently expressed recombination activity. To estimate the degree of CSR that might occur at recall, we quantified the frequency of IgM to IgG2b circle transcripts [47] in 30-cell samples of antigen-specific $IgG2b^+$ B cells (**Fig. 7c-e**). There were few samples with transcripts (10-15%) detected at either day 3 of the early recall response in $GL7^+CD38^+$ IgG2b-switched antigen-specific B cells or by day 5 after recall in either $GL7^+CD38^+$ or $GL7^+CD38^-$ GC compartments of the draining LNs (**Fig. 7c-e**). Attesting to the sensitivity of this approach, >95% $GL7^+CD38^+$ IgG2b-expressing B cell samples from early in the primary response expressed IgM to IgG2b CSR activity. Taken together, this suggests that pre-existing switched-memory B cells, and not IgM^+ memory B cells, are the dominant antigen-specific precursors of secondary GC reactions.

DISCUSSION

In these studies, we develop a novel and high-fidelity means for connecting cellular phenotype, gene expression and BCR repertoire for the individual progeny of antigen-

specific memory B cells after antigen recall. Our findings establish the capacity of memory B cell responders to re-diversify expressed antigen-specific BCR in secondary GC reactions. In this manner, 'memory BCR re-diversification' can contribute substantially to the evolution of circulating antibody repertoires. *Cd83* and *Polh* gene expression segregated individual switched-memory GC B cells across four stages of GC function at the clonal and sub-clonal level. Assortment and progress of sub-clonal GC B cell activity described divergent adaptive evolutionary dynamics that simultaneously enhance antigen binding and drive intra-clonal diversity at the boost.

At the single cell level, switched-memory BCR re-diversification is supported by GC-specific transcriptional programs and driven by antigen-specific selection [9, 11, 14, 15]. The primary-response GC microenvironment and GC-specific transcriptional programs are required for induction of high-affinity switched B cell memory and central to antibody-based immune protection [3-5, 12]. Here, we probe the secondary GC transcriptional program at the single cell level and find individual class-switched GC B cells in four major clusters. Importantly, segregation of *Cd83* and *Polh* expression in single cells predicts the cyclic progression of GC function.

CD83 is associated with antigen presentation and stabilization of MHC II [42] and both protein and mRNA are differentially expressed in LZ GC B cells [3, 9]. Differential antigen uptake, presentation and up-regulation of molecules at the T-B interface by LZ Stage 1 & 2 GC B cells could facilitate antigen-specific selection. Higher-affinity LZ B cells could preferentially form longer productive contacts with GC T_{FH} cells [14], increase c-Myc expression [48, 49], re-enter the DZ [9] and undergo more rounds of division [15]. However, static analysis cannot resolve time of recruitment and phenotype-based isolation of cells cannot resolve cyclic re-entry dynamics. *Polh* is an error-prone DNA polymerase [41] differentially expressed in DZ GC B cells [9] to introduce point mutations in the expressed BCR. We find substantial fractions of individual *Polh*$^+$ GC B cells still expressing *Cd83* mRNA. This *Cd83*$^+$*Polh*$^+$ GC B cell subset up-regulates *Aicda*, *Pcna* and *Mki67* associated with somatic hypermutation and proliferation. Increased *Cxcr4* and decreased *Cxcr5* serve *to* relocate these cells to the GC DZ [11] (Stage 3). Extended DZ activities in *Cd83*$^-$*Polh*$^+$ GC B cells (Stage 4) involved decreased *cMyc* and *Pcna* expression with continued high levels of *Mki67* and *Cxcr4*. Hence, distinct changes in *Cd83* and *Polh* expression at the single cell level may further delineate DZ re-entry from ongoing BCR re-diversification as components of separable DZ GC B cell programs.

Under conditions of local protein vaccination and antigen recall, we demonstrate that switched-memory B cells can form robust secondary GC reactions. These findings are consistent with early reports of substantial non-PC antigen-specific cellular expansion [36, 37] and GL7$^+$ GC B cell emergence to recall [38]. Particulate antigens with IV priming [23, 24] engage splenic B cells by potentially different mechanisms, with varying cognate T_{FH} cell requirements and memory T_H cell induction. An altered balance of memory B cell subsets [35] may also impact the function of transferred memory B cells. Pre-immune repertoires of antigen-specific B cell and T_H cell responses to any foreign antigen will impact initial priming and potentially alter the recall response. In this manner, intact memory responses to phycoerythrin (PE) [21, 23] may be more sensitive to initial priming and adjuvant for the

formation of memory T_H and B cell compartments. Nevertheless, even after adoptive transfer, there is evidence for secondary GC formation by class-switched memory B cells [22, 25, 35], albeit at very low levels compared with PC production. Population based studies focused on changes in somatic hypermutation after transfer and recall [34] also supported ongoing switched BCR diversification.

Modifying switched-memory B cell fate at recall provides a powerful opportunity to optimize circulating antibody repertoires towards enhanced antigen binding. Skewing towards PC formation at recall has been attributed to transcriptional differences in switched versus IgM^+ memory B cells [25]. This skewing has also been seen in the PE-specific [21], VLP recall responses [24] and after SRBC recall in adoptive transfers [23]. We have observed rapid PC skewing in early splenic recall responses [36, 38]. Some of these differences can be attributed to the vaccine adjuvant skewing towards different memory B cell subsets [35]. It is also important to emphasize that memory B cell responses to most protein antigens require cognate T cell help [50]. Hence, we predict it will be plausible and advantageous to re-formulate the boost adjuvant to favor the secondary GC B cell fate and promote optimal switched antibody repertoires binding for effective long-lasting antigen-specific immunity.

We propose that complex viral proteins at infection [26, 27, 29, 30, 32] or in vaccine prime-boost formulation [28, 31, 33] will drive similar local BCR re-diversification mechanisms. Hence, ongoing changes to circulating antibody repertoires reported across many human infectious responses are most simply explained by the induction of local secondary GC reactions. Clusters of recently-diversified post secondary GC memory B cells and PCs in the circulation would be responsible for the ongoing clonal diversification observed in these human studies.

By targeting minimal epitopes on complex immunogens, we reveal divergent evolutionary dynamics at the polyclonal, clonal and sub-clonal levels in intact primed animals. At the population level, induced BCR changes converge towards higher-affinity binding of antigen [3, 4, 12]. However, at the single cell level, the reinforcement and expansion of multiple sub-clonal variants describes a more divergent evolutionary process. Under these conditions, recall responses to variant antigens would permit and then enhance re-focusing of memory BCR to antigenic variants of the original vaccine These powerful evolutionary mechanisms can rapidly remodel antibody repertoires of pre-existing memory B cells to optimize antibody-based immune protection. We propose that targeting switched-memory B cells to re-initiate GC specific transcriptional programs will enhance the depth and increase the breadth of vaccine-induced immune protection.

Methods

Mice

B6 (C57BL/6J), B6.CD45.1 (B6.SJL-$Ptprc^a$ $Pepc^b$/BoyJ), B6.$Rag1^{-/-}$ (B6.129S7-$Rag1^{tm1Mom}$/J), B6.MD4 (C57BL/6-Tg(IghelMD4)4Ccg/J) mice were bred and housed in pathogen-free conditions at The Scripps Research Institute. The Scripps Research Institutional Animal Care and Use Committee approved all experiments.

Immunizations and antibody treatments

Primary immunizations were performed with 400μg 4-hydroxy-3-nitrophenylacetyl (Biosearch) conjugated to keyhole limpet hemocyanin (Pierce, NP-KLH) mixed with MPL-based adjuvant subcutaneously at the base of the tail. Secondary immunizations (boosts) were subcutaneous or i.v. with 100μg NP-KLH in the absence (PBS only, soluble) or presence of MPL-based adjuvant greater than 70 days after priming. Immunization with Alum adjuvant (Aluminum-potassium-sulfate (Sigma) precipitated with 1M potassium hydroxide (Sigma)) and Complete Freund's Adjuvant (CFA, Sigma) was used as indicated.

To ablate persisting GCs in primed animals, anti-CD40L (MR1, BioXCell) blocking antibody was injected 3 times every other day (300μg per injection, i.p.) starting on week 9 after priming. Mice were sacrificed or boosted 6 days after the last injection. Matching doses of polyclonal hamster IgG (Pierce) were used as control.

Flow cytometry

Single cell suspensions of draining (inguinal and periaortic), non-draining (cervical) lymph nodes and spleen were prepared, incubation in 0.17M NH_4Cl to lyse red blood cells, cells were then counted and re-suspended in PBS with 5% (v/v) FBS at a concentration of 4×10^8 cells per ml for staining. Anti-CD16/32 (2.4G2) was first added for 10min on ice, before addition of cocktails of fluorophore-labeled or biotin-labeled monoclonal antibodies for 45 min on ice. After washing, biotin-labeled antibodies were revealed with Qdot655-streptavidin conjugates for 15 min on ice,

For surface IgG2b staining, cells were blocked with anti-CD16/32, incubated with biotinylated or PE anti-mouse IgG2b for 45 min on ice, washed and blocked with 1% mouse and rat sera, and then stained with a cocktail containing fluorophore-conjugated antibodies, NP-PE or NP-APC, and Qdot655-streptavidin for 45 min on ice. For intracellular Bcl-6 staining, surface-stained cells were labeled with the eFluor506 or eFluor780 viability dyes (eBioscience), fixed and permeabilized with buffers from a transcription factor staining kit (eBioscience), blocked with 1% mouse and rat sera in permeabilization buffer, and stained for 30 min on ice with PE anti-Bcl-6. A list of monoclonal antibodies used for this study is provided as Supplementary Table 1. Cells were washed and resuspended in PBS/FBS.

High-resolution analysis using a four laser Aria III with index cell sorting was central to all studies. Use of 12-15 color resolution for analysis and isolation of single class-switched antigen-specific GC B cells provided the requisite purity as attested by efficiency of single cell gene expression. Analysis was done on a FACS Aria III with FACS Diva software equipped with index sorting software (BD Biosciences) to record the exact data for each single cell sorted into each well of a 96 well plate. Indexed cell sorting permitted the direct tracking of individual cells processed for surface phenotype, BCR repertoire analysis and gene expression to quantify the levels and penetrance frequency for genes of GC-associated function. Flow cytometry data were analyzed with FlowJo software (Tree Star).

Fluorescence immunohistochemistry

Draining lymph nodes were fixed overnight at 4°C in paraformaldehyde-lysine-periodate buffer, dehydrated in 30% sucrose, embedded in OCT medium (Tissue-Tek) and frozen on dry ice. Eight micrometer tissue sections were prepared and slides were air dried then rehydrated in PBS prior to staining. Sections were permeabilized and blocked for 1h at room temperature in NGS blocking buffer (PBS + 10% normal goat serum + 0.05% Triton X-100). Purified rat monoclonal antibodies (anti-AID or anti-CD4) were diluted in NGS blocking buffer and added on slides for overnight incubation at 4°C in a humidified chamber. Washed slides were then stained with AlexaFluor488 goat anti-rat IgG diluted in NGS blocking buffer for 1 hour at room temperature. Slides were then blocked with NRS blocking buffer (PBS + 10% normal rat serum + 0.05% Triton X-100) before staining with fluorophore-conjugated antibodies diluted in NRS blocking buffer overnight at 4°C. A list of antibodies used is in Supplementary Table 1. Slides were mounted in Aquamount medium (Thermo Scientific) and analyzed on a Nikon C2 confocal microscope equipped with 4 lasers (408nm, 488nm, 543nm, 633nm) and a 60x objective. Images were acquired with Nikon Elements software and further processed with Adobe Photoshop CS4.

Single-cell multiplex quantitative PCR and BCR analysis

Individual LNs were collected for most integrated studies of GC function to increase likelihood of clonal samples. Single NP-specific B cells ($CD3^-$ $Gr1^-$ $CD19^+$ IgD^- IgM^- $\lambda1^+$ NP^+) GC ($CD138^-$ $B220^+$ $CD38^-$ $GL7^+$) or memory cells ($CD138^-$ $B220^+$ $CD38^+$ $GL7^-$) were individually FACS sorted into 96 well plates containing 5μL RT-Pre-Amplification Master Mix (2.5μL CellsDirect 2x Reaction Mix; 0.1μL SuperScript III RT/Platinum Taq (CellsDirect One-Step qRT-PCR kit, Invitrogen); 0.25μL pooled 0.5μM outside gene expression primers and VLλ1 and VH186.2 BCR outside primers; 2.15μL DEPC DDW). As negative control for each plate, at least 4 wells per plate had no cell and were processed throughout the procedure. Therefore a total of 384 individual negative data points were included for each plate. The RT was performed at 50°C for 15 min, followed by 95°C for 2 min, then 22 cycles of 95°C for 15 sec, 60°C for 4 min. The pre-amplified cDNA were diluted 5 times in TE buffer and processed for gene expression and B cell receptor analysis.

For multiplex gene expression analysis, the BioMark Real-time PCR system (Fluidigm) was used with TaqMan Universal PCR Master Mix (Applied Biosystems) and inventoried TaqMan gene expression assay in 96.96 dynamic arrays. Single cells not expressing at least 2 reference genes (*Gapdh*, *Actb* and *B2m*) were removed from the analysis (<5% of cells). The Ct values from individual cells were transformed into relative mRNA abundance levels by subtracting the Ct value from a baseline of 30 and converting to numerical values at $2^{(30-Ct)}$ for display on log scale. Primers and Taqman assays used for RT qPCR are displayed in Supplementary Table 2.

For BCR analysis, 1μl of the pre-amp product was used for 10μl amplification reaction containing 2 u/ml Taq polymerase, 200μM of each dNTP (Roche), 1mM Tris-HCl, 1.5mM MgCl, 25mM KCl and 0.8μm of the nested primers VH186-b(sense) (5'-CTT GGC AGC AAC AGC TAC AG-3') and Cg1-b(antisense) (5'-CAC TGG CTC AGG GAA ATA GC-3') for heavy chain amplification with the following PCR program: 95°C for 5 min then

40 cycles of 95°C for 15 sec, 55°C for 45 sec, 72°C for 90 sec, ending with 72°C for 5 min. PCR products were purified (ExoSAPT-IT, USB) and sequenced with Big Dye Terminator v3.1 cycle sequencing kit (Applied Biosystems) using 3.2pmol of the second round PCR antisense primer Cg1-b for heavy chain products. Sequence products were purified (BigDye XTerminator purification kit, Applied Biosystems) and run on a 3130 genetic analyzer (Applied Biosystems). V, D and J gene segments were assigned using NCBI Ig blast and the Kabat nomenclature. Single cells nucleotide sequence were near-neighbor aligned using Clustal Omega and based on nucleotide sequence in BCR junctional regions assigned a clone and cell ID. Phylogenetic trees were generated with Dendroscope 3 [39].

t-distributed stochastic neighbor embedding (t-SNE)

For gating and visualization, gene expression data files were compiled into FCS files (CsvtoFcs, GenePattern, Broad Institute) and analyzed with FlowJo. t-SNE [40] analysis of gene expression (30-Ct format) from GC B cells (n=372) was done with Cyt (Pe'er lab, Columbia University) running with Matlab, with 7 selected parameters (*Aicda*, *Bcl6*, *Cd79b*, *Cd83*, *Cxcr4*, *Mki67*, *Polh*). t-SNE creates a two-dimensional representation of data points where closest neighbors in the high dimensional space are plotted in close proximity, thus conserving the local similarities between data points. The t-SNE coordinates of every data point were collated to the transformed ($2^{30\text{-}Ct}$) gene expression parameters and other sequence-derived parameters (e.g. clonal identity) into a new FCS file. Four distinct subsets were defined on the t-SNE map (stages 1-4). Cells which were in none of these gates were assigned a GC stage based on their expression of *Cd83* and *Polh*, and are marked with an asterisk or represented by a colored ball without black contour. For every gene in our dataset (n=87), we used a Mann-Whitney test to compare the expression (30-Ct) by single cells of consecutive t-SNE-defined stages. The expression index (E.I.) of every gene was calculated for the four stages as: E.I. = “percent of positive cells” x “mean expression of positive cells”. For every gene, the fold change in expression between consecutive stages was calculated as: and depicted as ± depending on the direction of change. “Volcano” plots were then created for every transition by plotting the p-value of the Mann-Whitney comparisons versus the fold change for every gene. Genes that had a fold change >1.5 (gain or loss) and a $p<0.05$ for at least one of the transitions were selected, and the fold changes of every transition were displayed in a heatmap (Gene-E, Broad Institute).

Adoptive transfers

Single cell suspensions pooled from spleen and draining lymph nodes of primed donor animals (B6 or B6.CD45.1) 10 weeks after NP-KLH immunizations were prepared. For transfer of non-specific class-switched memory B cells into B6.Rag1$^{-/-}$ recipients, cell suspensions were stained with a cocktail of monoclonal antibodies, and class-switched memory B cells ($CD8^-$ $Gr1^-$ IgM^- IgD^- $CD4^-$ $CD19^+$ $GL7^-$) and $CD4^+$ $CD44^{hi}$ ($CD8^-$ $Gr1^-$ IgM^- IgD^- $CD19^-$ $CD4^+$ $CD44^{hi}$) memory T cells were sorted separately into complete DMEM culture medium by FACS. Spleen cell suspensions from congenically marked B6.MD4 mice were prepared at the same time, and each recipient B6.Rag1$^{-/-}$ mouse was transferred i.p. with approximately 10^5 class-switched memory B cells, 7.5×10^5 $CD4^+$ $CD44^{hi}$ memory T cells, and 25×10^6 B6.MD4 spleen cells. Recipient mice were

immunized shortly after transfer with 100μg NP-KLH in MPL adjuvant i.p. (or adjuvant only). Donor B cell progeny was analyzed in recipient spleens 14 days after transfer.

For transfer of NP-specific memory B cell subsets, several enrichment strategies were used throughout the study to minimize cell sorting time. In some experiments, cell suspensions were first incubated with biotinylated anti-IgM (1B4B1, Southern Biotech) and anti-IgD (217-170, BD Biosciences), washed and mixed with streptavidin microbeads (Miltenyi) before purifying positive and negative fractions on magnetic columns (Miltenyi). Both fractions were stained with the same cocktail of monoclonal antibodies, and class-switched NP-specific memory B cells ($CD8^-$ $Gr1^-$ IgM^- IgD^- $CD4^-$ $CD19^+$ $GL7^-$ $CD38^+$ NP-PE^+) and $CD4^+$ $CD44^{hi}$ memory T cells ($CD8^-$ $Gr1^-$ IgM^- IgD^- $CD19^-$ $CD4^+$ $CD44^{hi}$) were sorted from the negative fractions by FACS, while IgM^+ NP-specific memory B cells ($CD8^-$ $Gr1^-$ IgM^+ IgD^+ $CD4^-$ $CD19^+$ $GL7^-$ $CD38^+$ NP-PE^+) were sorted from the positive fraction.

In other experiments, cell suspensions were first incubated with biotinylated anti-kappa light chain (187.1, BD Biosciences), anti-CD8 (53-6.7), anti-TER-119 (TER-119), anti-NK1.1 (PK136), anti-F4/80 (BM8) and anti-Gr1 (RB8-6C5, all from eBioscience), washed and mixed with Biotin Binder Dynabeads (Invitrogen) before separating the bound and unbound cells in a magnet. The negative unbound fraction was then stained with the cocktail of monoclonal antibodies and all subsets were sorted from that fraction based on the phenotypes described above.

Regardless of the enrichment method used, purity of sorted populations was greater than 99% upon re-analysis. Approximately $3\text{-}5 \times 10^3$ NP-specific memory B cells (class-switched or IgM^+) and $5\text{-}10 \times 10^5$ $CD4^+$ $CD44^{hi}$ memory T cells were transferred i.v. (tail vein) into B6, B6.CD45.1, or B6.MD4 hosts. Shortly after transfer, recipient animals were immunized with a total of 100μg NP-KLH in adjuvant (50μg i.p and 50μg s.c. base of tail). Donor B cell progeny was analyzed in recipient spleens 7 days after transfer. There was no significant impact of different enrichment procedures on the outcome of these experiments.

Analysis of *Cμ-Iγ2b* circle transcripts

$IgG2b^+$ NP-specific B cells expressing different levels of CD38 and GL7 from day 5 after priming or days 3 and 5 after boost (adjuvant) were isolated. Thirty cell samples were sorted for pre-amplification in a 5μl master mix as described above with 50nM external forward (Iγ2b F1, 5’-GCT CCA CAT GTG AGT GTG GT-3’) and reverse (Cμ R1, 5’-GCG AGG TGG CTA GGT ACT TG-3’) primers [47]. 96-well thermocyclers (Applied Biosystems) were used for cDNA synthesis and *Cμ-Iγ2b* circle transcript pre-amplification: 15 min at 50°C, 2 min at 95°C, and 22 cycles of 15 sec at 95°C followed by 4 min at 60°C. Pre-amplification products were diluted 1:5 in TE buffer, and 1μl was used for amplification of *Gapdh* and *Cμ-Iγ2b* circle transcript cDNA by quantitative PCR (qPCR). The reaction mix consisted of 5μl SYBR green reaction mix (PerfeCTa SYBR Green FastMix, Quanta Biosciences), 250nM internal forward (Iγ2b F3, 5’-CAC TGG GCC TTT CCA GAA CTA-3’, or Gapdh F, 5’-GCAG TGG CAA AGT GGA GAT T-3’) and reverse (Cμ R3, 5’-AAT GGT GCT GGG CAG GAA GT-3’, or Gapdh R, 5’-TGC CGT GAG TGG AGT CAT AC-3’) primers, and 3.5μl water. MicroAmp Fast 96-well plates (Applied Biosystems) were used in a

StepOnePlus Real Time qPCR thermocycler with the following program: 10 min at 95°C, 40 cycles of 30 sec at 95°C followed by 1 min at 60°C, and melt curve generation by 0.3°C increments from 60°C to 95°C. *Gapdh* amplicons were detected with a Ct of approximately 25-30, and *C*μ-*Iγ2b* circle transcripts at a Ct of 13-16. Products were run on a 2% (w/v) agarose gel to verify they matched the expected amplicon sizes (approximately 90 bp for *Gapdh* and 300 bp for *C*μ-*Iγ2b*). While *Gapdh* transcripts were detected in all samples sorted, *C*μ-*Iγ2b* circle transcripts had a "digital" expression; thus positive samples had at least 1 out of 30 sorted cells that had recently switched from IgM to IgG2b, but negative samples likely contained none.

Statistics

Mean values, standard error of the mean, unpaired t-tests and Mann-Whitney tests were calculated and graphed with Prism software (GraphPad). A P value of less than 0.05 was considered statistically significant.

Supplementary Material

Refer to Web version on PubMed Central for supplementary material.

Acknowledgements

P.J.M. was supported by a Young Investigator Award from the Foundation Bettencourt-Schueller. S.L.O received fellowships from the Swiss National Science Foundation, the Novartis Jubliaeumsstiftung and the Roche Research Foundation. Grants from the National Institutes of Health supported the work (AI047231, AI040215 and AI071182 to M.G.M-W.). This is TSRI manuscript #26086.

References

1. Crotty S. Follicular helper CD4 T cells (TFH). Annu Rev Immunol. 2011; 29:621–663. [PubMed: 21314428]
2. Fazilleau N, Mark L, McHeyzer-Williams LJ, McHeyzer-Williams MG. Follicular helper T cells: lineage and location. Immunity. 2009; 30:324–335. [PubMed: 19303387]
3. Victora GD, Nussenzweig MC. Germinal centers. Annu Rev Immunol. 2012; 30:429–457. [PubMed: 22224772]
4. MacLennan IC. Germinal centers. Annu Rev Immunol. 1994; 12:117–139. [PubMed: 8011279]
5. McHeyzer-Williams M, Okitsu S, Wang N, McHeyzer-Williams L. Molecular programming of B cell memory. Nat Rev Immunol. 2012; 12:24–34. [PubMed: 22158414]
6. Allen CD, Okada T, Tang HL, Cyster JG. Imaging of germinal center selection events during affinity maturation. Science. 2007; 315:528–531. [PubMed: 17185562]
7. Hauser AE, et al. Definition of germinal-center B cell migration in vivo reveals predominant intrazonal circulation patterns. Immunity. 2007; 26:655–667. [PubMed: 17509908]
8. Schwickert TA, et al. In vivo imaging of germinal centres reveals a dynamic open structure. Nature. 2007; 446:83–87. [PubMed: 17268470]
9. Victora GD, et al. Germinal center dynamics revealed by multiphoton microscopy with a photoactivatable fluorescent reporter. Cell. 2010; 143:592–605. [PubMed: 21074050]
10. Shulman Z, et al. T follicular helper cell dynamics in germinal centers. Science. 2013; 341:673–677. [PubMed: 23887872]
11. Bannard O, et al. Germinal center centroblasts transition to a centrocyte phenotype according to a timed program and depend on the dark zone for effective selection. Immunity. 2013; 39:912–924. [PubMed: 24184055]

12. Rajewsky K. Clonal selection and learning in the antibody system. Nature. 1996; 381:751–758. [PubMed: 8657279]
13. Muramatsu M, et al. Class switch recombination and hypermutation require activation-induced cytidine deaminase (AID), a potential RNA editing enzyme. Cell. 2000; 102:553–563. [PubMed: 11007474]
14. Shulman Z, et al. Dynamic signaling by T follicular helper cells during germinal center B cell selection. Science. 2014; 345:1058–1062. [PubMed: 25170154]
15. Gitlin AD, Shulman Z, Nussenzweig MC. Clonal selection in the germinal centre by regulated proliferation and hypermutation. Nature. 2014; 509:637–640. [PubMed: 24805232]
16. Berek C, Berger A, Apel M. Maturation of the immune response in germinal centers. Cell. 1991; 67:1121–1129. [PubMed: 1760840]
17. Jacob J, Kelsoe G, Rajewsky K, Weiss U. Intraclonal generation of antibody mutants in germinal centres. Nature. 1991; 354:389–392. [PubMed: 1956400]
18. Allen D, et al. Timing, genetic requirements and functional consequences of somatic hypermutation during B-cell development. Immunol Rev. 1987; 96:5–22. [PubMed: 3298009]
19. Berek C, Milstein C. Mutation drift and repertoire shift in the maturation of the immune response. Immunol Rev. 1987; 96:23–41. [PubMed: 3298007]
20. Siekevitz M, Kocks C, Rajewsky K, Dildrop R. Analysis of somatic mutation and class switching in naive and memory B cells generating adoptive primary and secondary responses. Cell. 1987; 48:757–770. [PubMed: 3493076]
21. Benson MJ, et al. Distinction of the memory B cell response to cognate antigen versus bystander inflammatory signals. The Journal of experimental medicine. 2009; 206:2013–2025. [PubMed: 19703988]
22. Pape KA, Taylor JJ, Maul RW, Gearhart PJ, Jenkins MK. Different B cell populations mediate early and late memory during an endogenous immune response. Science. 2011; 331:1203–1207. [PubMed: 21310965]
23. Dogan I, et al. Multiple layers of B cell memory with different effector functions. Nature immunology. 2009; 10:1292–1299. [PubMed: 19855380]
24. Zabel F, et al. Viral particles drive rapid differentiation of memory B cells into secondary plasma cells producing increased levels of antibodies. J Immunol. 2014; 192:5499–5508. [PubMed: 24821969]
25. Kometani K, et al. Repression of the transcription factor Bach2 contributes to predisposition of IgG1 memory B cells toward plasma cell differentiation. Immunity. 2013; 39:136–147. [PubMed: 23850379]
26. Corti D, Lanzavecchia A. Broadly neutralizing antiviral antibodies. Annu Rev Immunol. 2013; 31:705–742. [PubMed: 23330954]
27. Gao F, et al. Cooperation of B cell lineages in induction of HIV-1-broadly neutralizing antibodies. Cell. 2014; 158:481–491. [PubMed: 25065977]
28. Jiang N, et al. Lineage structure of the human antibody repertoire in response to influenza vaccination. Science translational medicine. 2013; 5:171ra119.
29. Klein F, et al. Somatic mutations of the immunoglobulin framework are generally required for broad and potent HIV-1 neutralization. Cell. 2013; 153:126–138. [PubMed: 23540694]
30. Liao HX, et al. Co-evolution of a broadly neutralizing HIV-1 antibody and founder virus. Nature. 2013; 496:469–476. [PubMed: 23552890]
31. Vollmers C, Sit RV, Weinstein JA, Dekker CL, Quake SR. Genetic measurement of memory B-cell recall using antibody repertoire sequencing. Proceedings of the National Academy of Sciences of the United States of America. 2013; 110:13463–13468. [PubMed: 23898164]
32. West AP Jr. et al. Structural insights on the role of antibodies in HIV-1 vaccine and therapy. Cell. 2014; 156:633–648. [PubMed: 24529371]
33. Wrammert J, et al. Rapid cloning of high-affinity human monoclonal antibodies against influenza virus. Nature. 2008; 453:667–671. [PubMed: 18449194]

34. Kaji T, et al. Both mutated and unmutated memory B cells accumulate mutations in the course of the secondary response and develop a new antibody repertoire optimally adapted to the secondary stimulus. Int Immunol. 2013; 25:683–695. [PubMed: 24021876]
35. Zuccarino-Catania GV, et al. CD80 and PD-L2 define functionally distinct memory B cell subsets that are independent of antibody isotype. Nature immunology. 2014; 15:631–637. [PubMed: 24880458]
36. McHeyzer-Williams LJ, Cool M, McHeyzer-Williams MG. Antigen-specific B cell memory: expression and replenishment of a novel b220(−) memory b cell compartment. The Journal of experimental medicine. 2000; 191:1149–1166. [PubMed: 10748233]
37. McHeyzer-Williams MG, Nossal GJ, Lalor PA. Molecular characterization of single memory B cells. Nature. 1991; 350:502–505. [PubMed: 2014051]
38. Shapiro-Shelef M, et al. Blimp-1 is required for the formation of immunoglobulin secreting plasma cells and pre-plasma memory B cells. Immunity. 2003; 19:607–620. [PubMed: 14563324]
39. Huson DH, Scornavacca C. Dendroscope 3: an interactive tool for rooted phylogenetic trees and networks. Syst Biol. 2012; 61:1061–1067. [PubMed: 22780991]
40. Amir el AD, et al. viSNE enables visualization of high dimensional single-cell data and reveals phenotypic heterogeneity of leukemia. Nat Biotechnol. 2013; 31:545–552. [PubMed: 23685480]
41. Delbos F, Aoufouchi S, Faili A, Weill JC, Reynaud CA. DNA polymerase eta is the sole contributor of A/T modifications during immunoglobulin gene hypermutation in the mouse. The Journal of experimental medicine. 2007; 204:17–23. [PubMed: 17190840]
42. Tze LE, et al. CD83 increases MHC II and CD86 on dendritic cells by opposing IL-10-driven MARCH1-mediated ubiquitination and degradation. The Journal of experimental medicine. 2011; 208:149–165. [PubMed: 21220452]
43. Kasturi SP, et al. Programming the magnitude and persistence of antibody responses with innate immunity. Nature. 2011; 470:543–547. [PubMed: 21350488]
44. Schwickert TA, Alabyev B, Manser T, Nussenzweig MC. Germinal center reutilization by newly activated B cells. The Journal of experimental medicine. 2009; 206:2907–2914. [PubMed: 19934021]
45. Kaji T, et al. Distinct cellular pathways select germline-encoded and somatically mutated antibodies into immunological memory. The Journal of experimental medicine. 2012; 209:2079–2097. [PubMed: 23027924]
46. Taylor JJ, Pape KA, Jenkins MK. A germinal center-independent pathway generates unswitched memory B cells early in the primary response. The Journal of experimental medicine. 2012; 209:597–606. [PubMed: 22370719]
47. Kinoshita K, Harigai M, Fagarasan S, Muramatsu M, Honjo T. A hallmark of active class switch recombination: transcripts directed by I promoters on looped-out circular DNAs. Proceedings of the National Academy of Sciences of the United States of America. 2001; 98:12620–12623. [PubMed: 11606740]
48. Calado DP, et al. The cell-cycle regulator c-Myc is essential for the formation and maintenance of germinal centers. Nature immunology. 2012; 13:1092–1100. [PubMed: 23001146]
49. Dominguez-Sola D, et al. The proto-oncogene MYC is required for selection in the germinal center and cyclic reentry. Nature immunology. 2012; 13:1083–1091. [PubMed: 23001145]
50. Aiba Y, et al. Preferential localization of IgG memory B cells adjacent to contracted germinal centers. Proceedings of the National Academy of Sciences of the United States of America. 2010; 107:12192–12197. [PubMed: 20547847]

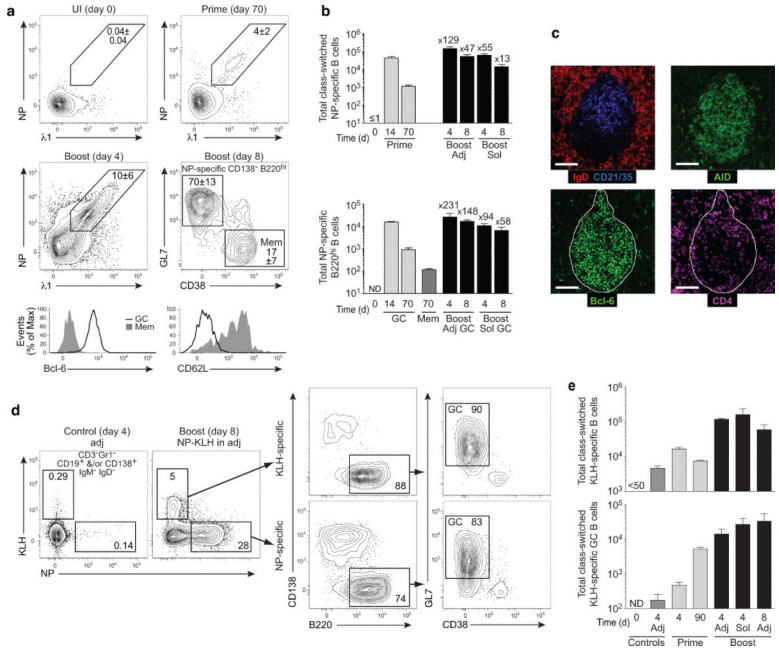

Figure 1. Switched-memory B cells form robust secondary germinal centers

(a) Representative flow cytometric analysis of class-switched ($IgM^{-}IgD^{-}$) antigen-specific ($\lambda1^{+}$ NP^{+}) B cells ($CD3^{-}Gr1^{-}CD19^{+}$) in draining lymph nodes before and 70 days after NP-KLH priming, 4 and 8 days after antigen boost with adjuvant, as indicated. Numbers in gates indicate mean ± sem percentage. Antigen-specific secondary GC B cells (CD38-$GL7^{+}$) express Bcl-6 and not CD62L. **(b)** Numbers of class-switched and GC phenotype antigen-specific B cells after prime and boost, with and without adjuvant. Bars graphs indicate mean ± sem (ND: not detected). The fold increase over day 70 memory cells is indicated above each boost condition (black bars). N = 5-10 individual mice for each timepoint. **(c)** Immunofluorescence for IgD, CD21/35, AID, Bcl6 and CD4 as indicated across two serial sections 8 days after soluble boost (50μm scale bar). **(d)** Flow cytometric analysis of KLH-specific B cells and NP-specific B cells in draining lymph nodes of adjuvant only primed control animals at day 4, and at day 8 after adjuvant NPKLH boost. GC B cells (B220+ CD138- CD38- GL7+) were identified as shown within KLH-specific (upper) and NP-specific (lower) class-switched B cells in boosted animals as indicated. Mean percent of parent gate is indicated. **(e)** Total class-switched KLH-specific B cells (upper) and KLH-specific GC B cells (lower) in draining lymph nodes of control animals (unimmunized or 4 days adjuvant only immunization) and NP-KLH immunized animals at the indicated days after prime or boost, with (adj) or without adjuvant (sol) for the boost. Bar graphs show mean ± sem (ND: not detected), n=3.

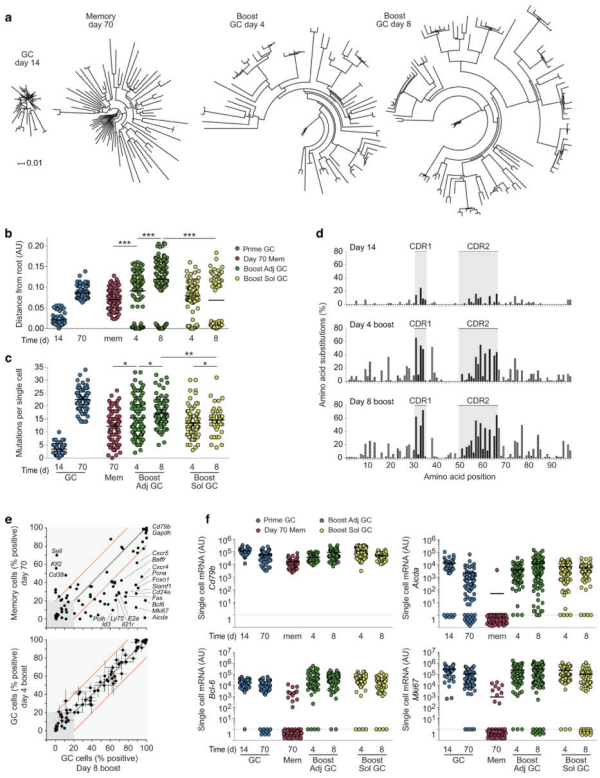

Figure 2. Switched BCR diversification and secondary GC transcription

C57BL/6 mice were immunized with NP-KLH in adjuvant and draining lymph nodes analyzed 14 and 70 days after priming and 4 and 8 days after antigen boost with adjuvant and without adjuvant (sol). Single class-switched ($IgD^{-}IgM^{-}$) antigen-specific specific ($\lambda1^{+}NP^{+}$) memory ($CD38^{+}GL7^{-}$) and GC ($CD38^{-}GL7^{+}$) B ($CD3^{-}Gr1^{-}CD19^{+}$ $B220^{+}$) cells were isolated for $V_H186.2$ focused BCR repertoire analysis and single cell multiplex qPCR. **(a)** Primary day 14 GC, day 70 memory, and GC cells day 4 and 8 following boost circular phylograms displaying near-neighbor sequence alignment and clonal relatedness (n=56; 75, 93 and 133 single cells respectively; same scale for each phylogram). Displayed is **(b)** distance from root sequence, **(c)** number of mutations per single cell (n=56, 83, 75, 110, 133, 89 and 60 respectively) and **(d)** aa substitutions across $V_H186.2$ gene segment. **(e)** Single cell 96-plex RT-qPCR on isolated antigen-specific memory and GC B cells with comparisons across populations for percent positive cells and **(f)** levels per cell using reference value of 30-C_T value converted as described in methods to establish baseline of 1.0 for all assays. (**b), (c)** and **(f)** each symbol represents signal from an individual cell, black bar indicates mean. *p<0.05 **p<0.01 ***p<0.001, Mann-Whitney test.

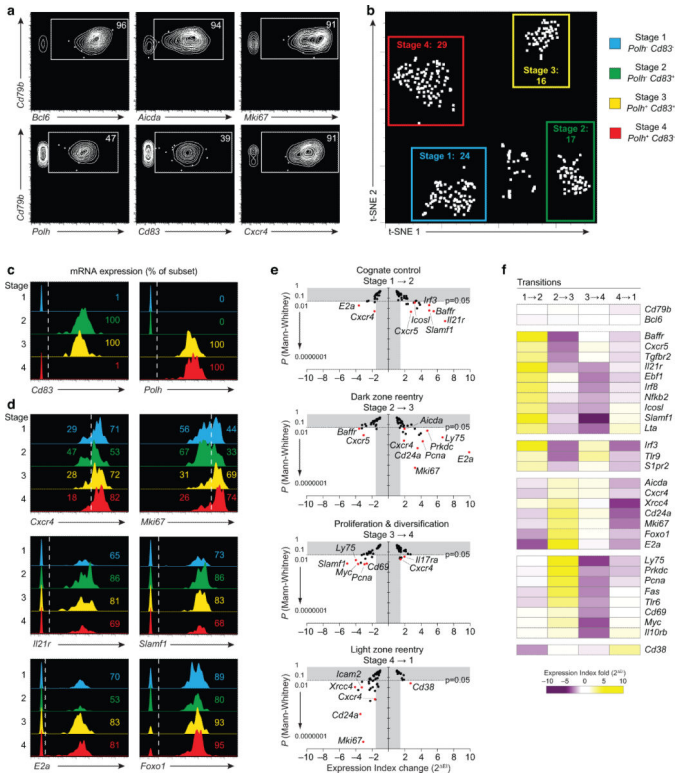

Figure 3. *Cd83* and *Polh* expression assorts four cyclic stages of GC activity

(a) Probability contours of single cell gene expression for *Cd79b*, *Bcl6*, *Aicda*, *Mki67*, *Polh*, *Cd83* and *Cxcr4* in GC B cells (day 4 and day 8, n=372). **(b)** These data are combined and clustered in a two-dimensional display using t-distributed stochastic neighbor embedding (t-SNE) that describes 4 major sub-groups labeled stage 1-4 that tightly overlap with **(c)** distribution of *Cd83* and *Polh*. **(d)** Distribution of *Cxcr4* and *Mki67* used for initial tSNE clustering and *Il21r*, *Slamf1*, *E2a* and *Foxo1* based on the t-SNE gates defined above. **(e)** "Volcano" plots highlighting the gene expression differences in successive t-SNE-defined stages according to their statistical significance (see details in Methods). **(f)** Heatmap representation of changes in gene expression for *Cd79b*, *Bcl6*, and select genes with an expression index change ≥1.5 and $p<0.05$ for that change in at least one of the transitions.

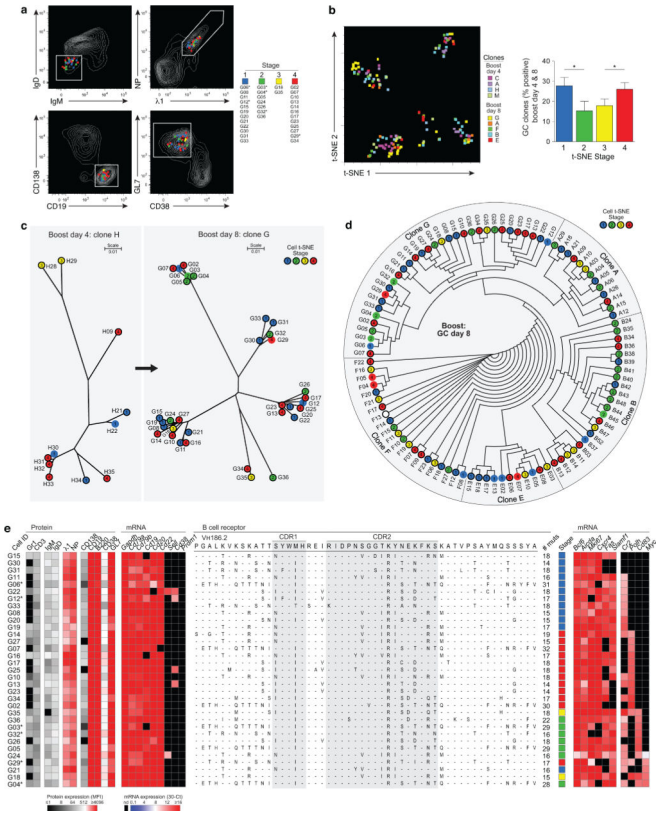

Figure 4. Adaptive radiation during sub-clonal BCR evolution in the GC

(a) Indexed cell sorting is depicted from day 8 boost ‘clone G’ as colored symbols for individual cells at different stages of the GC cycle overlaid on contour plots of total populations. **(b)** Distribution of individual cells from multiple clones from days 4 and 8 after the boost (with ≥10 members isolated) and summary of stage distribution. n=9 clones from 6 experiments, total single cells n=153. Bar graphs show mean ± sem, *p<0.05, t-test. **(c)** Radial phylograms for clones H and G and **(d)** summary dendrogram for all boost day 8 clones depicting the stage of GC cycle allocated to each member of the clone based on tSNE clustering. **(e)** Integrated analysis of protein levels (MFI), mRNA expression (30-C_T value) and V_H186.2 mutation pattern and t-SNE stage for individual GC cells from boost day 8 clone G (displayed in a-d).

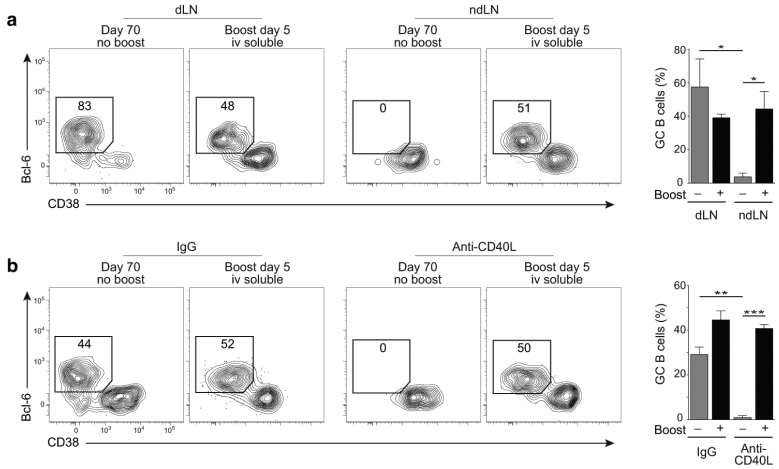

Figure 5. De novo secondary GC formation

(a) Mice were primed with NP-KLH in MPL adjuvant, rested for 70 days before boosting with soluble NP-KLH intravenously. Flow cytometric analysis of Bcl-6 and CD38 on NP-specific B cells (λ1+ NP+ B220+ CD138- class-switched B cells) in draining and non-draining (cervical) LN 5 days after boost. Bar graphs represent mean ± sem percentage Bcl-6^{+}CD38^{-} GC among λ1+ NP+ B220+ CD138- class-switched B cells before boost (day 70, grey bars) and 5 days after soluble boost (+, black bars) in the draining LN (dLN) and non-draining LN (ndLN). n=3 mice per group for each timepoint. *p<0.05, two-tailed t-test. **(b)** In NP-KLH primed mice, GC were ablated using anti-CD40L mAb (or controls treated with hamster IgG) one week before boosting with soluble NP-KLH intravenously. NP-specific B cells in spleen were analyzed by flow cytometry as in **(a)** before (day 70) and 5 days after boost in control or anti-CD40L treated animals. Box number indicates percent of parent population. Bar graphs represent mean ± sem percentage GC among λ1+ NP+ B220+ CD138- class-switched B cells before boost (day 70, grey bars) and 5 days after soluble boost (+, black bars) in the spleen of hamster IgG-treated (control) and anti-CD40L-treated animals. n=3 mice per group for each timepoint. **p<0.01, ***p<0.001, two-tailed t-test.

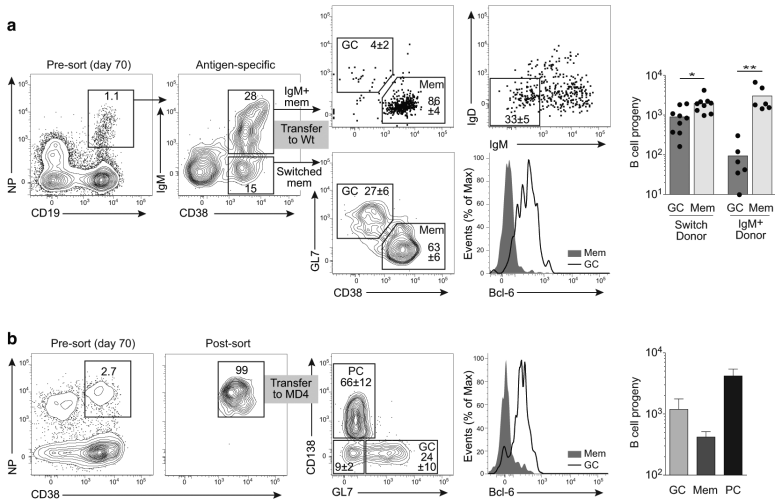

Figure 6. Switched-memory B cells can form secondary GC on transfer and recall

Sorted antigen-specific IgM$^+$ and class-switched memory B cells (NP+ CD138- B220+ CD19+ GL7- CD38+) were adoptively transferred into **(a)** naive WT congenic hosts and **(b)** naive B6.MD4 congenic hosts (class-switched group only) then recovered for analysis at day 7 after immunization with antigen in adjuvant. n=6 for IgM transfer, n=9 for class-switched memory transfer, mean±sem, **(a)** each symbol represents individual recipients *$p < 0.05$, **$p < 0.01$, two-tailed t-test.

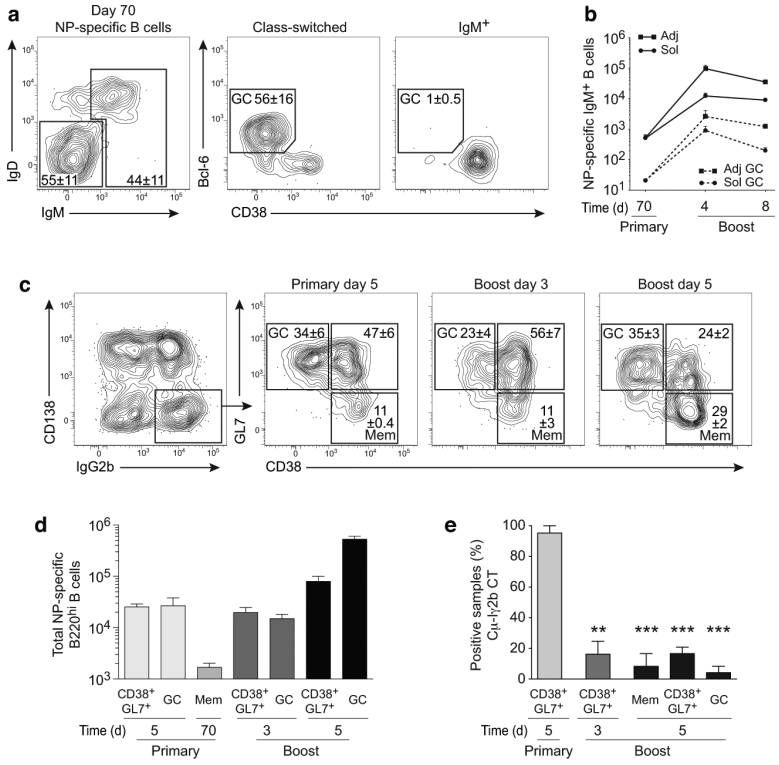

Figure 7. Switched-memory B cells are dominant precursors for secondary GC

(a) Representative flow cytometric analysis for IgM and IgD distribution in total NP-specific B cells (CD3- Gr1- CD138- CD19+ B220+ λ1+ NP+) (left), with representative Bcl-6 and CD38 expression among class-switched (middle) and IgM+ (right) NP-specific memory B cells in draining LN 70 days after NP-KLH priming. Numbers in gates indicate mean ± sem percentage. n=3. **(b)** Total IgM+ NP-specific B cells (solid lines, CD3- Gr1- CD19+ or CD138+ λ1+ NP+ IgM+) and NP-specific GC B cells (dashed lines, CD138- B220+ CD38- GL7+) per draining LN at the indicated days after priming and boost with NP-KLH with (Adj, square) or without (Sol, circle) adjuvant. n=3 mice for each timepoint. **(c)** Sorted IgG2b+ NP-specific B cells from draining lymph nodes 5 days after primary and day 3 and 5 secondary (boost) immunization with NP-KLH in adjuvant. Three subsets of IgG2b+ NP-specific B cells (CD3-Gr1-CD19+IgD-NP+ CD138- IgG2b+) were defined based on CD38 and GL7 expression. Box indicates percentage, mean ± sem, n=3 for each timepoint. **(d)** Total class-switched NP-specific B220+ (CD3- Gr1- CD138- IgM- IgD- CD19+ B220+ NP+) B cells subsets (CD38+ GL7+, GC and memory, gated as in Figure1A) in draining LN at the indicated days after priming (Primary) or boosting (Boost) with NP-KLH in adjuvant. Bars indicate mean ± sem. n = 3-9 individual mice for each timepoint. **(e)** Assessment of recent class-switch recombination from IgM to IgG2b by PCR amplification of Cμ-Iγ2b circle transcripts in sorted 30-cell samples of the indicated subsets. Three separate experiments with a total of 12-20 samples for each phenotype and timepoint were pooled and summarized, showing the percentage of samples positive for Cμ-Iγ2b circle transcripts. Graph displays mean ± sem, n=3 mice for each timepoint, ** $p<0.01$, *** $p<0.001$, two-tailed t-test.